SHOCK-WAVE SYSTEM ANALYSIS FOR COMPRESSION-DECOMPRESSION RAMP FLOW

Maxim Loginov[‡]

Nikolaus A. Adams[*]

Alexander A. Zheltovodov[†]

[*]Lehrstuhl für Aerodynamik,
Technische Universität München
Boltzmannstr. 15, D-85748 Garching, Germany
nikolaus.adams@tum.de
[†]Khristianovich Institute of Theoretical and Applied Mechanics,
Russian Academy of Sciences, Siberian Branch,
Novosibirsk 630090, Russia

ABSTRACT

Well-resolved Large-Eddy Simulations (LES) are performed in order to investigate flow phenomena and turbulence structure of the turbulent boundary layer along a supersonic compression-decompression ramp. The simulations reproduce directly a reference experiment with a free-stream Mach number of $Ma_\infty = 2.95$ and a Reynolds number based on the incoming boundary-layer thickness of $Re_{\delta_0} = 63560$. An analysis of the results shows a good agreement with the reference experiment in terms of mean quantities and turbulence structure. The computational data confirm theoretical and experimental results on fluctuation-amplification across the interaction region. In the wake of the main shock a shedding of shocklets is observed which are annihilated subsequently by the expansion near the decompression corner. The development of large-scale streamwise vortices in the vicinity of the successive compression and decompression corners is analyzed and support for a Görtler-like generation mechanism is provided.

INTRODUCTION

For the investigation of perturbed supersonic turbulent boundary layers a range of canonical flow configurations (Knight *et al.*, 2003) are commonly employed. Most of these configurations impose a single type of perturbation on the flow. In many practical configurations, however, more than one perturbation event may occur. For instance, for the compression-decompression ramp a rapid compression by the shock wave is followed by an expansion fan (Zheltovodov, 2006), often before the compressed boundary layer has relaxed to an turbulence equilibrium.

In this paper we extend the work of Loginov *et al.* (2006), where only the compression corner was considered. One objective of the current numerical investigation is a direct comparison with an available experiment for the compression-decompression ramp flow. Accordingly, all flow parameters and the flow geometry are matched to the experiment (Zheltovodov and Yakovlev, 1986; Borisov *et al.*, 1993): the free-stream Mach number is $Ma_\infty = 2.95$, the Reynolds number based on the incoming boundary-layer thickness is $Re_{\delta_0} = 63560$, the ramp deflection angle is $\beta = 25°$. Our simulation results have been validated against the experimental data, and the validity of the employed simulation approach for such flows has been demonstrated (Loginov *et al.*, 2006). A large scale shock motion was observed as a contribution to the overall unsteady shock-system behavior, whereas traveling shocklets, identified from the simulation data, were found to provide an additional mechanism for turbulence amplification in the wake of the main compression shock. Also the existence of streamwise Görtler-type vortices was corroborated numerically and a relaminarization tendency in the separation region was found.

EXPERIMENTAL SETUP

The experiments were performed at the Institute of Theoretical and Applied Mechanics (Novosibirsk, Russia) in the T-352 wind tunnel with a test-section size of 200 × 200mm. A ramp with step height of $h^* = 6$mm was placed on a flat plate at the distance of 157mm from the leading edge and at an deflection angle of 25° (Zheltovodov and Yakovlev, 1986). Here and in the following dimensional lengths are indicated by an asterisk. Reference length is the mean undisturbed boundary-layer thickness of $\delta_0^* = 2.27$mm (the computational value of δ_0 differs by 4 % (Loginov *et al.*, 2006)). A sand-paper strip near the leading edge is used to initiate transition to turbulence. The model surface is expected to be adiabatic in the mean, which is achieved by running the wind tunnel for some time before measurements are taken. The experimental data provide, among others, the mean wall pressure distribution, the mean velocity profiles, root-mean-square profiles of mass-flux, density and velocity fluctuations at several downstream stations (Zheltovodov and Yakovlev, 1986). The positions of the stations in terms of the downstream coordinate measured along the wall from the compression corner position, are given in table 1. Mean skin-friction measurements were performed by the Global Interferometry Skin Friction technique (GISF) which has an estimated accuracy of 6–10 % (Borisov *et al.*, 1993). An experimentally obtained flow field structure together with the measurement stations E1-E5 are sketched in figure 1. The separation shock formed by the deflected surface constitutes the forward leg of a λ-shock configuration above the separation zone. The expansion fan near the decompression corner encounters compression waves in the boundary layer near the surface (Zheltovodov and Yakovlev, 1986).

Symbol	$x_1^*, [mm]$	x_1
E1	-35.	-15.42
E2	10.	4.41
E3	18.	7.93
E4	34.	14.98
E5	59.	25.99

Table 1: Streamwise distance of the measurement stations for forward facing steps with $\beta = 25°$.

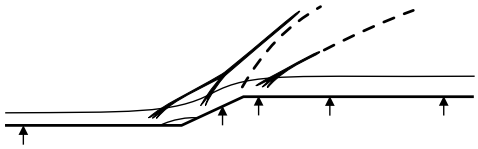

Figure 1: Sketch of flow structure and measurement stations.

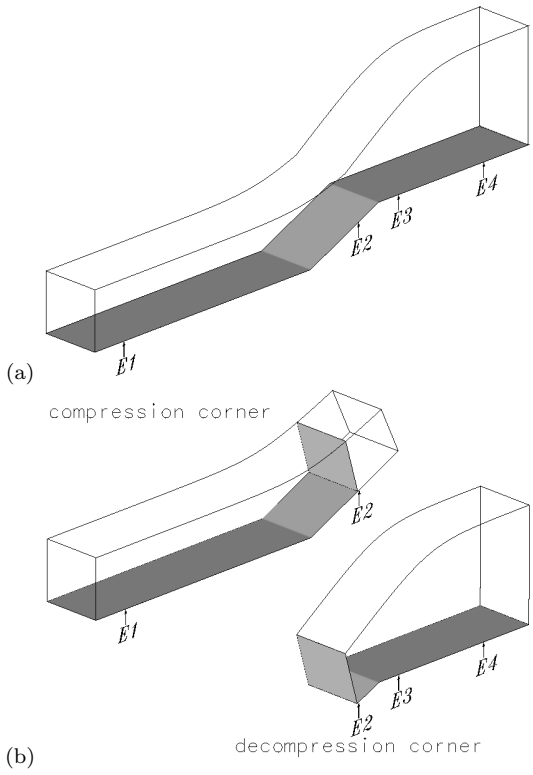

Figure 2: Split domain.

SIMULATION METHOD

Domain and grid

Based on previous experience it was estimated that a well-resolved LES for the full configuration requires about 29 million gridpoints. For this reason the domain of the full test configuration (figure 2a) was split into two parts, namely the compression and the decompression corner part, as shown in figure 2(b), and two separate simulations were performed. The domain size is chosen according to the reference experiment, the arrows denote the experimental reference stations E1-E4 (figure 1). The domain does not include the experimental station E5 since it would almost double the gridsize for the same resolution requirements. The compression-corner domain is continued beyond the decompression corner position ensuring that the outflow boundary condition does not affect the upstream flow. A possible upstream influence of the decompression corner is not taken into account for the compression-corner simulation. The inflow section of the decompression-corner domain is exactly matched to a cross-section of the compression-corner domain shown as shown in figure 2(b). Station E2 belongs to both domains, furthermore a short overlapping region of length $x_1 \approx 2$ exists, allowing for a cross-checking of both simulations in this region. The spanwise domain size is chosen wide enough so that large-scale coherent structures such as Görtler-like vortices can be captured (Loginov *et al.*, 2006). The domain of the second simulation, containing the decompression corner only, has the extent of $L_1 = 14.4x_1^*/\delta_0^*$ measured along the surface in the streamwise (x_1) direction, $L_2 = 4x_1^*/\delta_0^*$ in the spanwise (x_2) direction, and in the wall-normal (x_3) direction L_3 varies from $3.6x_1^*/\delta_0^*$ at inflow to $7.6x_1^*/\delta_0^*$. The computational mesh consists of $401 \times 132 \times 201$ points (about 10.6 million in total). The rather large domain height made it possible to avoid an influence of the upper boundary condition on the flow field near the triple point of the λ-configuration.

Numerical method

The approximate deconvolution model (ADM) is used for subgrid-scale modeling (Stolz *et al.*, 2001a; 2001b). The numerical method is the same as in previous simulations (Stolz *et al.*, 2001a; Loginov *et al.*, 2006): a 6th-order compact central finite-difference scheme (Lele, 1992) is used for discretizing all spatial derivatives, time advancement is done with an explicit low-storage 3rd-order Runge-Kutta scheme (Williamson, 1980). As inflow boundary conditions we prescribe all conservative variables as function of time, using data from a separate computation. For the compression-corner simulation results of a flat plate boundary layer calculation are used (Adams, 1998; Loginov *et al.*, 2006). Similarly, the instantaneous field of all conservative variables in a cross-section was saved 5033 times during a period of $259\delta_0/U_\infty$ of the compression-corner simulation and used as inflow conditions for the decompression corner. It is worthwhile to note that an essential temporal inhomogeneity of the inflow data caused by the shock-system unsteadiness does not permit the use of temporally periodic inflow conditions in the decompression-corner simulation. Periodic boundary conditions were applied in the spanwise direction. At the outflow a sponge-layer technique is used (Adams, 1998). At the upper truncation plane of the computational domain non-reflecting conditions are imposed. The wall is assumed to be isothermal with uniform temperature distribution in spanwise direction, along the streamwise direction it is taken from the experiment (Zheltovodov *et al.*, 1987; Loginov *et al.*, 2006), where the wall is supposed to be adiabatic. No-slip conditions are enforced on the velocity at the wall. Minor modifications of the boundary conditions in the decompression-corner simulation were made. In order to maintain numerical stability a second order Jameson-like (Jameson *et al.*, 1981) dissipation is added locally near the upper computational-domain boundary.

RESULTS

We discuss computational results for the full configuration, keeping in mind that two domains with overlapping regions are used. It should be noted that we cannot expect

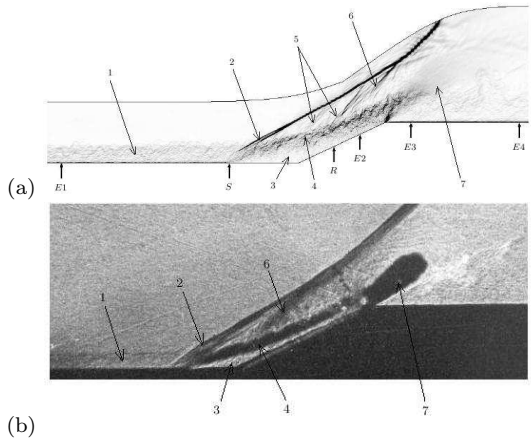

Figure 3: Instantaneous representation of the flow by a Schlieren-type visualization. The computed density gradient averaged in spanwise direction $\|\nabla\rho\|$ (a) and experimental Schlieren visualization (b). Long arrows indicate events discussed in the text.

an exact match of the results from both simulation in the overlapping region because of several reasons: (i) the explicit filter used in ADM depends on the grid, which does not match for the two domains in the overlap region; also the filter kernel at the domain boundary differs from that at interior points; (ii) the decompression corner data are affected by the time interpolation of the inflow-data, even though a small time spacing with an interval of $\Delta t_{in} \approx 0.05\delta_0/U_\infty$ is used for the inflow data; (iii) the compression corner simulation does not take into account the effect of the decompression corner, which was substituted by an outflow sponge-layer condition; the estimated upstream distance affected by the decompression corner is about δ_0 (Loginov *et al.*, 2006). Also, the number of collected statistical samples are different in the simulations. The mean flow for the decompression corner is computed from 105 samples taken with an interval of $\Delta t \approx 0.5\delta_0/U_\infty$, while in the compression corner 1272 samples are taken. Thus, the results of the compression-corner simulation are more reliable in the overlapping region, excluding distance of about δ_0 upstream from decompression corner. In the following, the Reynolds averaged values are denoted as $\langle f\rangle = f' + f$ and Favre averaged as $\{f\} = \langle\rho f\rangle / \langle\rho\rangle = f + f''$

Mean flow and turbulence

An instantaneous snapshot of the computed Schlieren-type visualization (figure 3a) can be compared with an experimental picture (3b). The incoming boundary layer (1) encounters the compression by the ramp, giving rise to the main separation shock (2), i.e. the front leg of a λ-shock. The interaction results in flow separation (3) contained by a detached shear layer (4). In the wake of the separation shock the shedding of shocklets (5) can be observed. The reattachment shock, i.e. rear leg of the λ-shock, is highly unsteady (Loginov *et al.*, 2006) and clearly visible only in time-averaged visualizations. The boundary layer increases in thickness downstream of the expansion (7). Turbulent fluctuations are damped in the expansion fan downstream of the decompression corner, where also shocklets cannot be identified anymore. The separation (S) and reattachment (R) locations, determined from zero mean skin-friction averaged in spanwise direction, are indicated by arrows together with experimental stations positions.

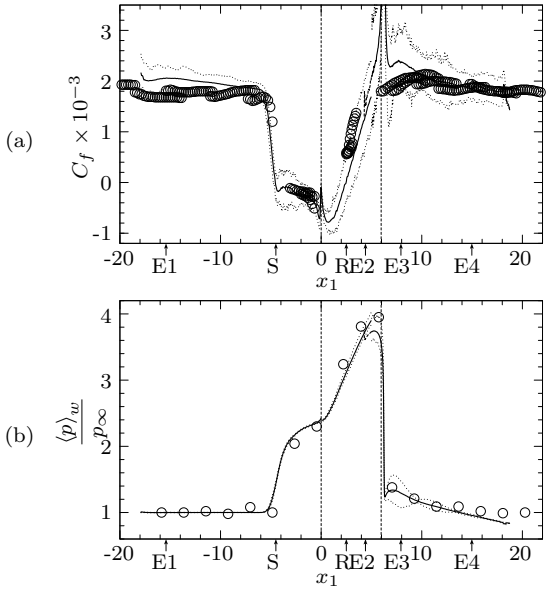

Figure 4: Averaged skin-friction coefficient (a) and wall-pressure (b) distributions in the streamwise direction. ∘ , reference experiment; ——— , current LES averaged in time and over spanwise direction; ····· , current LES averaged in time only, min and max values over spanwise; - - - - , decompression corner simulation results in the overlapping part of the domains. Symbols E1-E4 point to the experimental positions, S and R are separation and reattachment positions. The leftmost dashed vertical line indicates the compression-corner position and the right-most dashed vertical line the decompression-corner.

The mean skin-friction exhibits the typical behavior for separated flow (figure 4a). It should be noted that the temporal average of the skin-friction coefficient have some spanwise variation (dotted lines), spanwise and temporal average are in close agreement with the experiment (open circles). Some discrepancies in the overlap region are described earlier. An overshoot of C_f near the expansion corner is due to limited numerical resolution of the corner singularity. The wall pressure, normalized to its value in station E1, shows a plateau within the separation region, typical for non-small Reynolds numbers (figure 4b). A slight pressure increase in the region $6 < x_1 < 7$ may indicate the existence of a weak compression waves inside the boundary layer downstream of the expansion, as sketched in figure 1, which have been reported for experiment at larger deflection angles of $\beta = 45°$ (Zheltovodov *et al.*, 1983,). The destruction of streamwise vortices causes a higher spanwise variation of the wall pressure in this region.

Figure 5 gives an impression of the mean-velocity-profile evolution in the streamwise direction. The velocity deficit at station E2 is compensated by the expansion, and the profiles become fuller at station E3. Generally, the computed profiles agree well with the experimental data. A difference outside of the boundary layer at station E2 ($x_3 > 1$) may be attributed to a deficiency of the experimental measurement technique. For a more detailed analysis of velocity profiles within the separation region the reader is referred to Loginov *et al.* (2006).

The spanwise variation of the time-averaged C_f is shown in figure 6. The reason for this spanwise variation is dis-

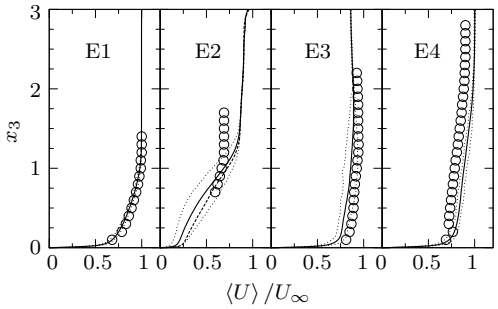

Figure 5: Velocity profiles at stations E1-E4. ∘ , reference experiment; ——— , current LES averaged in time and over spanwise direction; ····· , current LES averaged in time only, min and max values over spanwise; - - - - , decompression corner simulation results in the overlapping part of the domains.

cussed by Loginov *et al.* (2006). The skin-friction-coefficient variation decreases from $\pm 0.69 \times 10^{-3}$ at station E2 to $\pm 0.56 \times 10^{-3}$ at station E3. The maxima and minima, corresponding to divergence and convergence lines of the Görtler-like vortices, become less pronounced. Further downstream at station E4 the variation reduces further towards the undisturbed value ($\pm 0.25 \times 10^{-3}$). This reduced variation is an indication for the decay of the Görtler-like vortices when passing through the expansion. No longitudinal vortical structures can be identified after the decompression by common vortex identification criteria. The decay shortly downstream of the decompression corner observed in the simulation is in agreement with experimentally observed oil-flow pattern.

By Loginov *et al.* (2006) Görtler-like streamwise vortices have been identified and visualized. Here we provide additional evidence for the existence of such vortices by analyzing an effective Görtler number for the mean flow. If the mean streamline curvature in the separation region or in the reattachment region is larger than the critical value for laminar flow a mechanism for generating streamwise vortices very similar to that for laminar flow may be active in the turbulent flow as well. Tani (1962) suggested that the Görtler criterion can also be applied to turbulent flows by using the same characteristic length scale, δ_2, and by replacing the molecular viscosity ν by the eddy viscosity ν_T. If we assume that the eddy viscosity in the outer layer is given by $\nu_T = 0.018 U_\infty \delta_1$ then the Görtler number for a turbulent

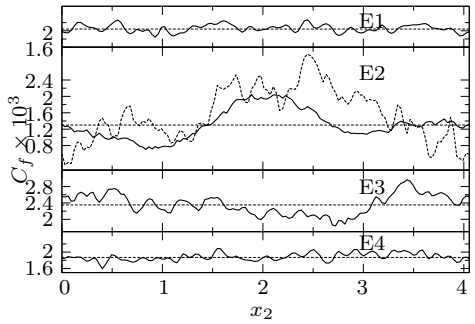

Figure 6: Distribution of the mean skin-friction coefficient at the wall in spanwise direction. ——— , averaged in time; - - - - , averaged in time and over spanwise direction; - - - - , decompression corner simulation results in the overlapping part of the domains.

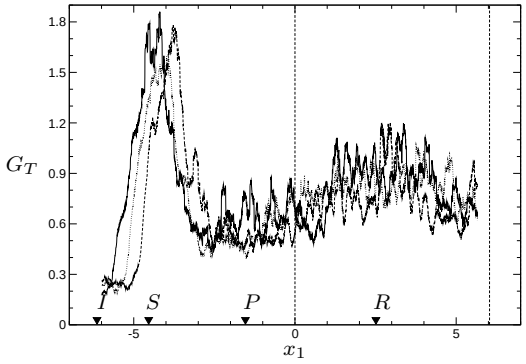

Figure 7: Görtler number distribution in streamwise direction. ——— , for streamline at $x_3 = 0.2$; ····· , for streamline at $x_3 = 0.4$; - - - - , for streamline at $x_3 = 0.6$

boundary layer can be estimated as

$$G_T = \frac{\delta_2}{0.018 \delta_1} \sqrt{\frac{\delta_2}{R}}. \quad (1)$$

Root-mean-square (RMS) values of the longitudinal mass-flux RMS(ρU), density RMS(ρ), and velocity RMS(U) fluctuations are shown at several downstream stations E1-E4 in figure 8 (top to bottom). The profiles are normalized with the respective maxima within the undisturbed boundary layer in order to comply with the experiment of Zheltovodov and Yakovlev (1986). In agreement with the experiment the RMS values increase during the interaction with the shock (see station E2) shifting the maximum from a near wall position to the detached shear layer. The Prandtl-Meyer expansion moves the maximum further away from the wall and damps the RMS values. Fluctuations are rather large outside of the boundary layer. Obviously the RMS profiles at the downstream station E4 have a different shape than for the equilibrium boundary layer on the flat plate (station E1). In particular a higher turbulence level can be noted in the outer flow ($x_3 > 2.6$). The agreement with the experimental data is good, some discrepancies at station E2 are discussed by Loginov *et al.* (2006) and Loginov (2006). The near-wall peaks which are well-resolved in the simulation are not captured by the experiment.

The streamwise evolution of the mass-flux fluctuation within the boundary layer and within the external flow is compared with the reference experiment in figure 9. For the fluctuation evolution within the boundary layer, maxima are taken from the boundary-layer fluctuation profiles, whereas for the evolution within the exterior flow maxima are taken from the exterior flow (refer to figure 8a). The data are normalized with their respective values at station E1. The results within the boundary layer show a good agreement with the experiment. The fluctuations are amplified by interaction with the shock at station E2 and damped subsequently by interaction with the expansion, at station E4 almost down to the initial level. For the exterior flow the turbulent fluctuations grow by an order of magnitude during the interaction with the shock. The expansion decreases this level, but it remains significantly higher than for the incoming flow over a long distance downstream. The simulation qualitatively follows this trend, a quantitative comparison is difficult due to the low level of external turbulence at station E1 which is used for normalization. An additional uncertainty is introduced by the ambiguity in determining the external flow with respect to the boundary layer in the

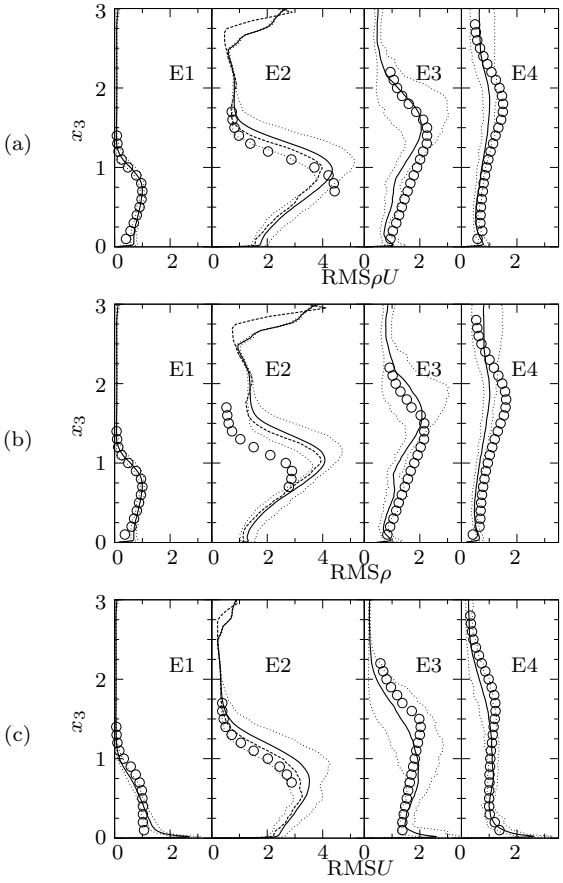

Figure 8: Root-mean-square profiles of the mass-flux (a), density (b) and velocity (c) fluctuations at stations E1-E4. ○ , reference experiment; ——— , current LES averaged in time and over spanwise direction; ····· , current LES averaged in time only, min and max values over spanwise; - - - - , decompression corner simulation results in the overlapping part of the domains.

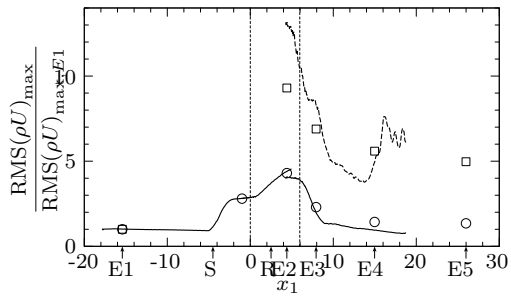

Figure 9: Relative changes of RMS of momentum fluctuations with streamwise direction. ——— , along the profile maxima within the boundary layer; - - - - , within the external flow; ○ , □ , reference experiment. The compression corner data were not analyzed for the external flow.

separation region. The observed behavior of turbulent fluctuations in the exterior flow can be explained as follows. Turbulence is amplified by the interaction with the shock wave, where shocklets also contribute to the enhancement of fluctuations. The expansion annihilates the shocklets as coherent structures, but does not damp entirely turbulent fluctuations caused by them, thus the external turbulence level remains high. This is an important finding of our LES with relevance to Reynolds-averaged turbulence modeling and wall-heat-flux prediction.

Shock system behavior

We find in the simulations a small-scale shock motion and a large-scale shock-motion (Loginov *et al.*, 2006). A series of instantaneous snapshots with a diamond marker in the field is shown in figure 10. Initially at $t = 180$ (subfigure *a*) the shock is located at the marker, then it moves upstream until it reaches its maximum upstream position at $t \approx 500$ (subfigure *c*). Finally the shock wave roughly recovers its initial position at $t = 691$ (subfigure *d*). Pressure-signal analysis allowed to identify the period of large-scale motion as about $686\delta_0/U_\infty$ or 1.5ms. The distance of the shock motion is about $1\delta_0$.

CONCLUSIONS

The numerical investigation of compression-decompression ramp flow was performed using large-eddy simulation. A high-Reynolds-number case corresponding to experimental conditions was considered, allowing for direct comparison. The results are validated successfully against the reference experiment. In particular a good agreement was achieved for surface-pressure and skin-friction distributions, mean velocity profiles, mass-flow, density and velocity fluctuations and distributions. The combined effect of perturbations sequentially imposed on turbulent boundary layer is investigated. It is shown that the expansion fan near the decompression corner destructs shocklets and streamwise vortices, while the level of turbulent fluctuation in the outer flow remains high.

ACKNOWLEDGMENTS

This research was founded by the German Research Council (DFG) through grant AD 186/1. Computing time was granted by the German National Supercomputing Center in Stuttgart (HLRS).

REFERENCES

N. A. Adams. Direct numerical simulation of turbulent compression corner flow. *Theor. Comp. Fluid Dyn.*, 12:109–129, 1998.

A. V. Borisov, S. S. Vorontsov, A. A. Zheltovodov, A. A. Pavlov, and S. I. Shpak. Development of experimental and computational methods of studies of supersonic separated flows. Preprint 9-93 ITAM, RAS SB, Novosibirsk, 1993. (in Russian).

A. Jameson, W. Schmidt, and E. Turkel. Numerical solution of the euler equations by finite volume methods using runge-kutta time-stepping schemes. Number 81-1259 in AIAA Paper. 1981.

D. D. Knight, H. Yan, A. G. Panaras, and A. A. Zheltovodov. Advances in CFD prediction of shock wave tur-

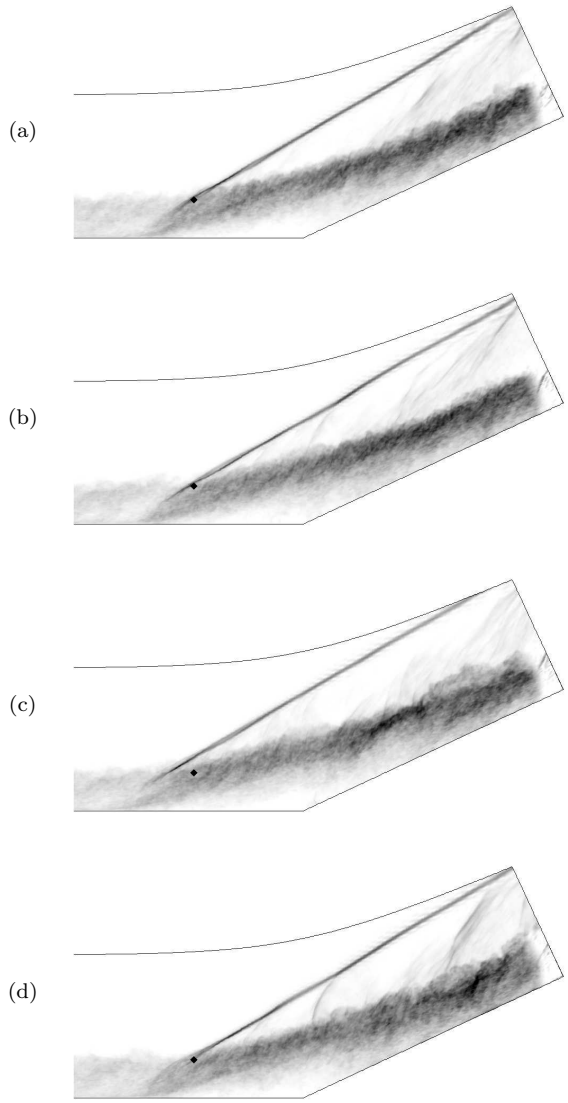

Figure 10: A series of instantaneous Schlieren-type visualizations. The time in subfigures (a) – (e) corresponds to $t = 180; 351; 518; 691$.

bulent boundary layer interactions. *Progress in Aerospace Sciences*, 39:121–184, 2003.

S. K. Lele. Compact Finite Difference Schemes with Spectral-like Resolution. *J. Comp. Phys.*, 103:16–42, 1992.

M. S. Loginov, N. A. Adams, and A. A. Zheltovodov. Large-eddy simulation of shock-wave/turbulent-boundary-layer interaction. *J. Fluid Mech.*, 565:135–169, 2006.

M. S. Loginov. *Large-eddy simulation of shock-wave/turbulent-boundary-layer interaction.* PhD thesis, Technical University of Munich, 2006.

S. Stolz, N. A. Adams, and L. Kleiser. The approximate deconvolution model for large-eddy simulation of compressible flows and its application to shock-turbulent-boundary-layer interaction. *Phys. Fluids*, 13:2985–3001, 2001.

S. Stolz, N. A. Adams, and L. Kleiser. An approximate deconvolution model for large-eddy simulation with application to incompressible wall-bounded flows. *Phys. Fluids*, 13:997–1015, 2001.

I. Tani. Production of longitudinal vortices in the boundary layer along a concave wall. *Journal of Geophysical Research*, 1962.

J. H. Williamson. Low-storage Runge-Kutta schemes. *J. Comput. Phys.*, 35:48–56, 1980.

A. A. Zheltovodov and V. N. Yakovlev. Stages of development, flowfield structure and turbulence characteristics of compressible separated flows in the vicinity of 2-D obstacles. Preprint 27–86 ITAM, USSR Academy of Sciences, Siberian Branch, Novosibirsk, 1986. (in Russian).

A. A. Zheltovodov, E. Schülein, and V. N. Yakovlev. Development of turbulent boundary layer under conditions of mixed interaction with shock and expansion waves. Preprint 28–83 ITAM, USSR Academy of Sciences, Siberian Branch, Novosibirsk, 1983. (in Russian).

A. A. Zheltovodov, E. G. Zaulichnyi, V. M. Trofimov, and V. N. Yakovlev. Investigation of heat transfer and turbulence in the compressible separated flows. Preprint 22–87 ITAM, USSR Academy of Sciences, Siberian Branch, Novosibirsk, 1987. (in Russian).

Zheltovodov. Some advances in research of shock wave turbulent boundary layer interactions. Number 06–0496 in AIAA Paper. 2006.